Available online at www.eccomasproceedia.org
Eccomas Proceedia COMPDYN (2017) 423-440

ECCOMAS
Proceedia

COMPDYN 2017
6th ECCOMAS Thematic Conference on
Computational Methods in Structural Dynamics and Earthquake Engineering
M. Papadrakakis, M. Fragiadakis (eds.)
Rhodes Island, Greece, 15–17 June 2017

On the Assessment of the Plaka Bridge Collapse using Non-linear Analysis Preventable or Doomed?

Nick Simos[1], George Manos[2], Evaggelos Kozikopoulos[2], Lambros Kotoulas[2]

[1]Brookhaven National laboratory
Upton, NY 11973, USA
simos@bnl.gov

[2]Lab. Strength of Materials and Structures
Aristotle University
Thessaloniki, Greece
gcmanos@civil.auth.gr

Abstract

The collapse of the historic Plaka Stone Bridge due to extreme flooding and in particular the pinpointing of the causes or possibly weak structural points that led to the structural failure is studied using high fidelity, three-dimensional non-linear numerical analysis and sensitivity studies. Specifically, the potential of a number of postulated scenarios in initiating failure and leading to the eventual collapse of the bridge are explored aided by sensitivity analyses relying on non-linear finite element modelling and is augmented by actual material properties of the structural elements deduced from laboratory tests following the collapse (i.e. stone and mortar). Presented in detail is the scenario which appears to closely replicate the mode of actual bridge failure observed (damage extend and debris distribution) and deemed by the authors to be most likely sequence of events that occurred. This scenario postulates the undermining of the central pier by support or shear section failure leading to large deformation and displacements on the lower part of the pier eventually leading to shear failure of the primary arch. Based on the failure mode predicted by simulation and corroborated with observed damage the vulnerability of the Plaka Bridge to this "*beyond design basis event*" even for an uncompromised structure is assessed by asking the question whether any preventive maintenance and upkeep could have saved this particular bridge or that its collapse was beyond human intervention.

Keywords: stone arch bridge; non-linear finite element analysis, section contacts, collapse

1. Introduction

Masonry arch bridges are an integral component of the heritage of cultures worldwide reflecting unique engineering techniques developed over the centuries starting from the Roman period and often characterizing the particular region where they are located. Variations in style and construction materials used, typically mortar and stone, help break down larger provinces into even smaller geographical regions, often groups of villages, which over the centuries adopted own unique styles depending on availability and access to construction materials. While in Roman times, for example, grand multi-arch bridges with economic and strategic importance were constructed under the orders of the empire, in rural,

Peer-review under responsibility of the organizing committee of COMPDYN 2017.
doi: 10.7712/120117.5430.18489

isolated communities, masonry stone bridges were constructed to serve local communities by utilizing construction materials from the immediate vicinity and therefore allowing the construction techniques to evolve and adopt to the quality of the available raw materials.

Plaka Bridge is an example of a bridge style developed in the Epirus province of north-western Greece, a mountainous region across with hundreds of stone bridges throughout of various styles representing localities and influenced by the availability of stone material. The bridge is at juncture of two renowned regions of stone construction known as Mastorohoria (villages of the stone masters) where magnificent stone structures were constructed with even poor stone quality and mortar and Zagori, a region rich in stone bridges constructed with higher quality and uniformity stone and mortar material. The Plaka Bridge, build in 1860s is influenced by both regions.

Because of age, neglect and compounded with often poor quality restoration works that were performed on these important monuments over the years, there is an urgent need to evaluate their current structural health state, identify structural degradation and locations of distress and perform appropriate restoration based on sound engineering assessment.

The recent collapse of the historic, renowned stone arch bridge of Plaka from extreme flooding and debris[1],[2] prompting questions of either (a) negligence in failing to address structural degradation or (b) urgent need to consider "beyond design basis events" for these structures (at least beyond what had been historically observed up to the time of construction) heightened awareness. It is not only the scientific challenges that the study of these non-linearly behaving structures present but also the need to identify the structural deficiencies and apply the most appropriate restoration.

In the last couple of decades experimental and numerical studies on masonry stone bridges have been performed to address both the ageing as well as the impact of vehicle or rail traffic both of which were not accounted for in the original construction. T. Akoi and co-workers [**3**] studied the Rakanji Bridge in Japan. Most relevant in this study is the fact that study conducted both stone and mortar tests establishing a good basis of analysis and material properties. Both micro-tremor measurement by ambient vibrations and acceleration by traffic vibrations were measured. Laboratory tests on similar materials to those of the bridge were conducted to establish the Young's modulus and compressive strength of the stone and the mortar. A number of historic stone arched bridges around Japan were studied by J. Kiyono and his co-workers [**4**]. In their all numerical study the dynamic behavior of several stone arched bridges were simulated using the 3-dimentional Distinct Element Method. Actual earthquake ground motions observed during the 1995 Hyogo-ken Nanbu earthquake were used in their study in conjunction with impulse waves to determine the modal characteristics and their collapse potential. B. Sevim and co-workers [**5**] conducted studies of arch bridges in Turkey where ambient vibration data were utilized to calibrate numerical models which subsequently were used to conduct linear earthquake analyses and assess the behavior of the bridges resulting from the excitation by the 1992 Erzincan Earthquake and address the importance of the model calibration process guided by actual field data. Numerical studies on the seismic behavior of the Konitsa Bridge (on the Aoos River near the city of Konitsa) which was build based on same principles and around the same time with Plaka Bridge were recently performed [**6**]. Addressing the effectiveness of restoration methodologies and options such as reinforcing concrete and/or pre-stressed steel jacket were evaluated base on numerical analysis.

Numerical studies of bridges and other stone and concrete structures of historical value have been performed in [**8-12**]. In these studies numerical techniques addressing the interaction of mortar and stone blocks or block-block non-linear contact were also explored. Specifically, B. O. Caglayan and co-workers [**8**] integrated a 3-D finite element analysis with in-situ acceleration measurements to study a long concrete arch bridge located in an earthquake-prone region of Turkey. Their calibrated bridge model was generated based on test results and numerical analysis was used in the structural capacity and

vulnerability assessment of the bridge structure. G.A. Drosopoulos [**9**] and co-workers studied the ultimate failure load of stone arch bridges based on 2-D, plane strain finite element analysis which included interfaces, simulation of cracks, unilateral friction contacts and the implementation of a path-following technique to estimate the ultimate load. Studies of other important masonry stone structures throughout Greece and relevant data bases are presented in [**10-12**]. Roman bridges are discussed in [13] and stone masonry bridges around Greece in [**14-15**].

The primary objective of this study is to identify, via a high fidelity numerical simulation representing the Plaka Bridge as a 3-D structure non-linear system and as close to its pre-collapse geometry as possible as well as acquiring representative structural material properties by testing elements of the structure itself, the most probable scenario of a "weak link" on the structure that led to its collapse during the "*beyond design basis event*". The underlying driver is, by corroborating the simulated collapse with actual evidence from the post-collapsed bridge, to hopefully identify the most-likely "weak link" and use the study as a guide/recommendation during the rebuilding phase of the bridge.

While a number of different scenarios of "*weak links*" in the structure were explored, the scenario of the of the undermining of the central pier structural integrity and in particular the experiencing of large displacements due to flood-induced degradation of its support on the river bed is presented in detail in this paper. This scenario and the subsequent collapse process was shown to be closest to the post-collapse field observations.

2. Plaka Bridge Location and Structural Characteristics

2.1 Location and Structural Details

The Plaka Bridge depicted in figure 13, one of the most spectacular stone masonry bridges was built in 1866 by the chief mason Kostas Mpekas and survived till January 2015 despite the structural damage that suffered during the World War II. It collapsed on the 2nd of February 2015 again from flooding of Arachtos River (Figures 14 and 15). The span of the main central arch was equal to 40m rising at a height of 20m. The total length of this bridge was over 60m and the width of the deck at mid-span of the central arch 3.20m.

As can be seen in Figure 3, a secondary arch is constructed at the right side of the main arch resulting in a mid-pier that is founded on the river bed. Moreover, a large arch shape opening is present at the left abutment with its foundation being also partly supported on the river bed. The presence of these two openings (right secondary arch and the left relief) was apparently insufficient to relieve the pressure load and protect the structure from the forces caused by this unprecedented flood.

What is important to note that updates of the original bridge shown in Figure 1 (left) introduced a more substantial parapet which add significant load to the structure which becomes top-heavy. It is a practice that has affected numerous such stone bridges without the consequences have been assessed properly.

Also to be noted in Figure 2 are the ties (or keys) that have been introduced on the primary arch only with a specific pattern. Reference to this point will be made later in the analysis.

Figure 1: Original Plaka Bridge structure (left) at the beginning of the 20th century and the bridge condition following bombardment during World War II (right). Notice the updated parapet on the right.

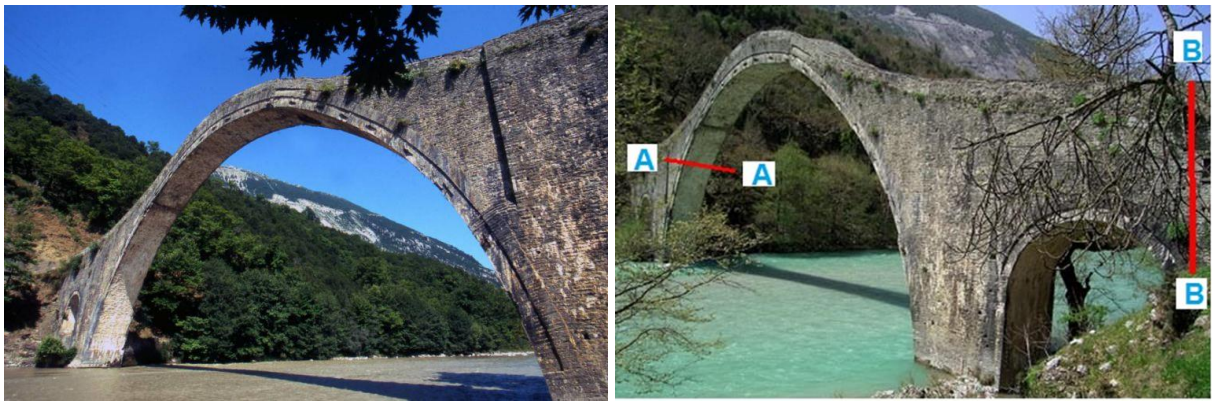

Figure 2: The Plaka Bridge prior to its collapse. Sown on the right is the location of the central pier (on the river bed) and its geometrical shape relative to the flow for assessing hydrodynamic forces. Designated as A-A and B-B are the failure surfaces/sections shown in Figure 3.

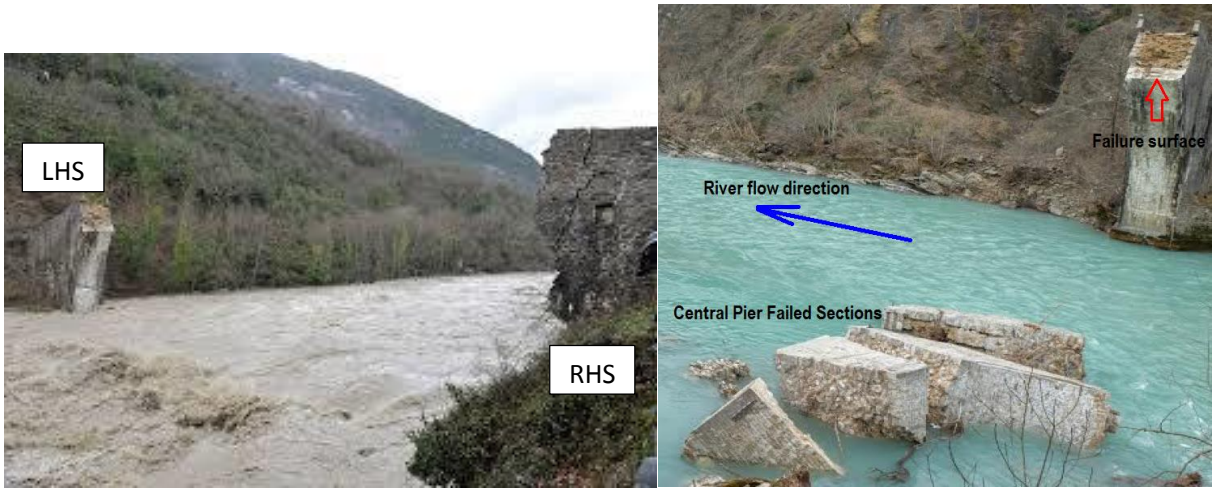

Figure 3: Post-collapse Plaka Bridge. Figure on the left provides some reference regarding the free stream velocity as well as the differential of water level between the upstream and downstream faces of the central pier. Shown on the right are the locations of the central pier segments/arch segments which

appear to have landed almost upstream and against the flow providing evidence that the bridge was not toppled over by the flow but rather collapsed in a more complicated manner.

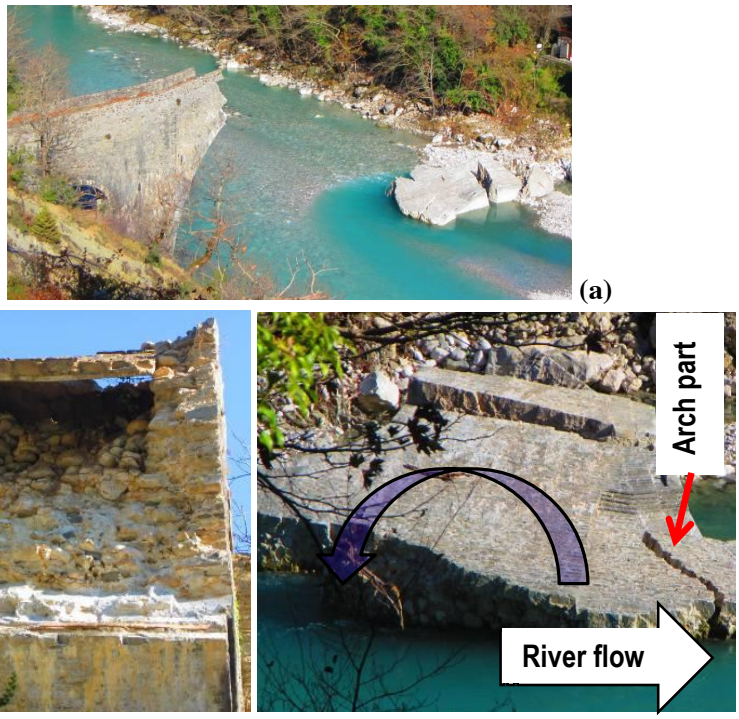

(a)

(b) (c)

Figure 4: Overview and details of the collapsed Plaka Bridge.

3. Material properties and Laboratory Tests

Construction material properties for the Plaka Bridge and other similar structures are expected to vary from region to region due to the inherent variability in the physical properties of the natural materials used from the immediate locality. Such variability will impact primarily the mortar used (composition, weathering, mechanical properties, etc.).

A laboratory testing sequence was performed with the objective to identify the mechanical characteristics of the basic materials representative of the materials employed to build stone masonry bridges in the general area. For this purpose, stone samples were selected from the vicinity of the collapsed Plaka Bridge and analyzed. Most importantly, it was facilitated that a mortar sample from the collapsed Plaka Bridge be taken to the laboratory for testing. From both the stone and mortar samples collected in-situ it was possible to form specimens of regular prismatic geometry. These specimens were subjected to either axial compression or four-point bending tests. For the compression tests the loaded surfaces of the prisms were properly cupped. Figure 6 depicts typical loading arrangements employed for the compression (stone and mortar specimens) tests employed for the Plaka Bridge samples. The applied load was measured through a load cell and the deformation of the tested specimens was measured employing a combination of displacement sensors as well as a number of strain gauges. These measurements were continuously recorded with a sampling frequency of 10Hz. Through these measurements, the mechanical characteristics of the tested specimens were obtained in terms of compressive strength, flexural tensile strength, Young's modulus of elasticity and Poisson's ratio. The obtained values of these mechanical parameters are listed in Tables 1-3.

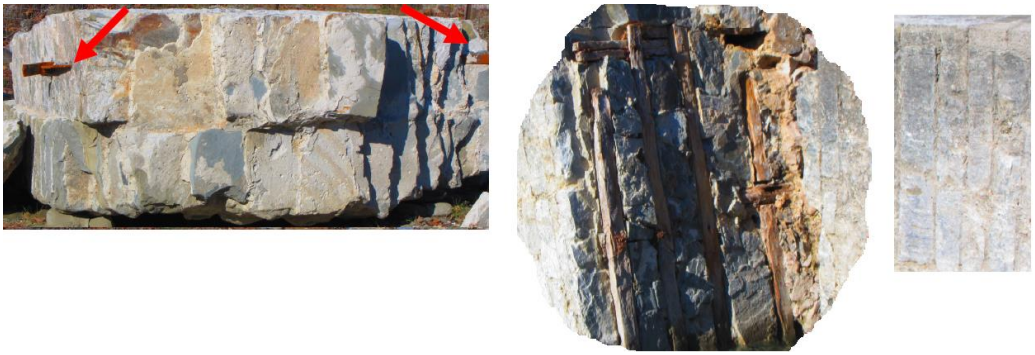

Figure 5: Plaka Bridge arch cross section exposed following the bridge collapse due to flooding

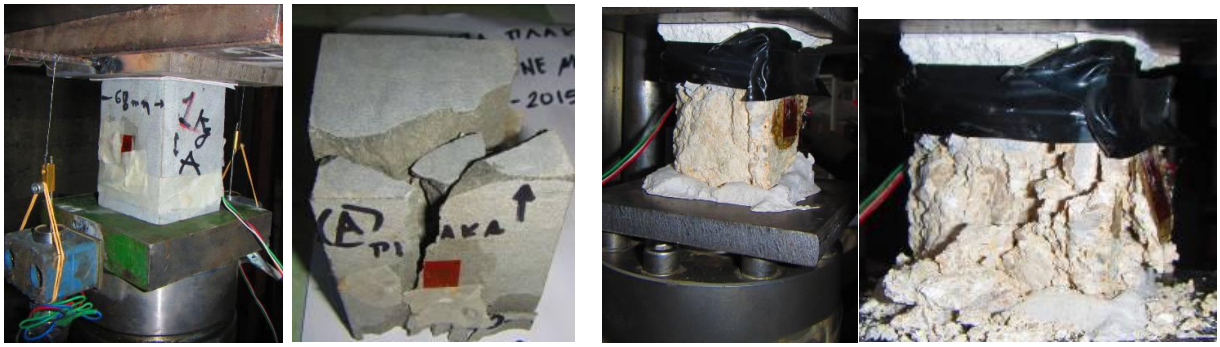

Figure 6: Testing in compression stone samples (left) and mortar samples (right) from Plaka Bridge

Table 1: Compression tests (12-18-2015) of stone samples from Plaka Bridge

Code Name of sample	Cross Section (mm2)	Height (mm)	Maximum load (KN)	Compressive Strength (MPa)	Slenderness ratio* / correction coefficient	Compressive Strength (MPa) with correction due to slenderness *
Specimen A	61.0 x 68.0	93.0	264.9	63.9	1.442 / 0.87	55.6
Specimen B	67.5 x 62.0	89.0	443.4	106.0	1.375 / 0.82	86.9
Plaka Bridge stone Specimens			**Average Compressive strength** = 71.3MPa, E_1=40000MPa, ν=0.142**			

* Reference slenderness ratio = 2.0.

** The average compressive strength refers to a prism with a slenderness ratio = 2

Table 2: Flexure tests (12-18-2015) of stone samples from Plaka Bridge

Code Name of sample	Width (mm)	Height (mm)	Span (mm)	Maximum Vertical load (KN)	Tensile strength (MPa)	Young's Modulus from flexure (MPa) (S.G.)
Specimen A	52.0	52.0	180.0	14.75	18.88	33330
Specimen B	52.0	52.0	180.0	12.13	15.52	36360
Plaka Bridge stone Specimens			**Average Tensile Flex. strength = 17.20MPa, E_2=34845MPa**			

Table 3: Compression tests (01-28-2016) of mortar samples from Plaka Bridge

Code Name of sample	Cross Section (mm2)	Height (mm)	Maximum load (KN)	Compressive Strength (MPa)	Slenderness ratio* / correction coefficient	Compressive Strength (MPa) with correction due to slenderness *
Specimen 1	27.5 x 57.0	66.0	3.228	2.06	1.562 / 0.91	1.875
Plaka Bridge mortar Specimens			**Compressive strength = 1.875MPa, E_1=2500MPa, ν=0.35**			

4. Finite element-based Simulation of Collapse of Plaka Bridge

Mechanical property values obtained from the stone and mortar sample tests revealed the following: The Young's modulus of the stone samples in axial compression has a value exceeding 40GPa whereas they yield a much less stiff behavior in flexure. It is well known that the complex tri-axial behavior of masonry cannot be easily approximated from the mechanical behavior of its constituents. For the studied stone masonry bridges this becomes even more difficult considering the various construction stages, the variability of the materials employed to form the distinct parts during these construction stages and the interconnection and contact conditions between the various parts formed during these construction stages (abutments, primary and secondary arch, deck, parapets, mandrel walls). Moreover, there is important information that is needed in order to form with some realism the boundary conditions at the river bed and bank. The lack of specific studies towards clarifying in a systematic way all these uncertainties represents a serious limitation in the numerical simulation process.

To enable damage/collapse of the Plaka Bridge associated with large deformations and separation of individual elements or whole sections a non-linear, 3D finite element model was developed and utilized. The nonlinearities introduced in the model captured both the material behavior and the interfaces between the different sections of the bridge (i.e. contact surfaces between primary and secondary arches, primary and secondary arch ends and foundation blocks, mandrel walls and secondary arch, etc.). Surface-to-surface and nodes-to-surface contact non-linear relations with possibility of separation were introduced at the interfaces between the various parts. Normal to the interface stresses and shear stresses (or forces in the case of nodes-to-surface contact) form the failure envelope governed by the relation

$$\left[\frac{\max(0.0,\sigma_{normal})}{\sigma_{fail}}\right]^2 + \left[\frac{\tau_{shear}}{\tau_{fail}}\right]^2 - 1 > 0$$

With σ_{normal} and τ_{shear} being the normal and shear stresses at the interface. This aims to represent the behavior and failure characteristics of the mortar between the parts. Following failure at the interface the parts will continue to be in contact acted upon compressive loads and will move apart under tensile loads.

The elements within each section utilized to discretize the volume are distinct and represented stone and mortar in a single element, in other words no block-to-block contact was implemented for the Plaka Bridge for this study due to the size of the problem and the excessive computational cost. Alternatively, mortar-stone was represented by "hybrid" element behavior in an effort to account for the role the mortar plays on the response of the structure and in particular when parts of the structure are experiencing tension and mortar representing the weakest link in the structure. The mortar-stone material was assumed to behave like "pseudo-concrete" according to the Winfrith model [16]. It is controlled by compressive and tensile strength as well as fracture energy and aggregate size. The compressive strength is considered to be controlled by the stone portion of the hybrid element (30 MPa) and the tensile strength by that of the mortar. The range of the tensile strength assumed in this study for the different sections of the Plaka Bridge is 0.25-2.1 MPa. The fracture energy (***FE***) assumed in the analysis dissipated in the opening of a tension crack was ***FE***=80 N/m. Upon formation of a tension crack no tensile load can be transferred across the crack faces. An additional failure criterion controlling the detachment of elements from the structure was introduced based on pressure (negative in tension). This criterion is used to simulate the behavior of mortar in the hybrid element which is considered to fail when the negative pressure exceeds a critical value. The pressure threshold assumed in the study was 1.1 MPa.

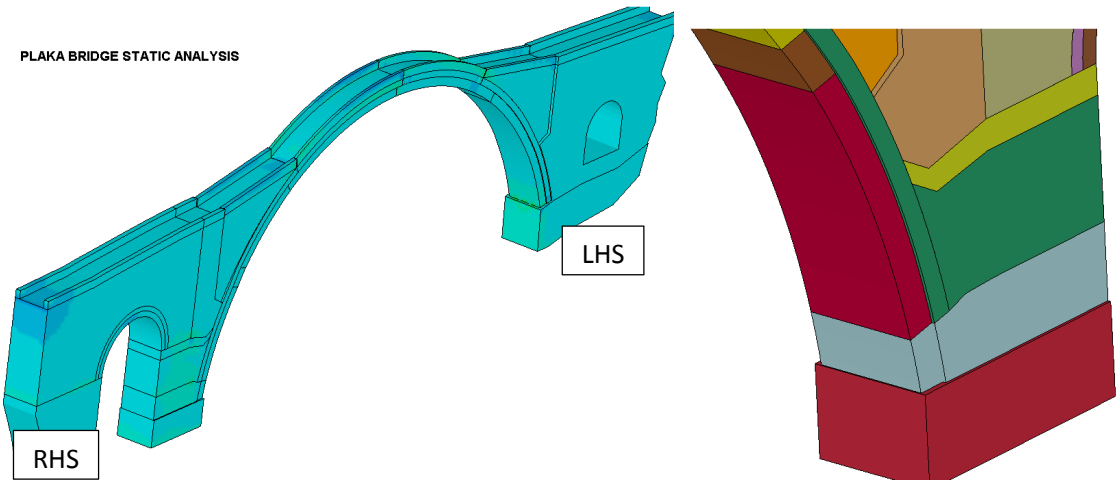

Figure 7: Global FEM representation of the Plaka Bridge (upstream side) at left and section details of the central pier.

Figure 7 depicts the modeled Plaka Bridge in 3-D along with details of the different sections that made up the structure. Interface (contact) conditions such as the one above control the structural continuity. These contact interfaces and their failure are controlled by the mortar between the distinct elements. Several failure conditions are available and have been explored in the study. The uncertainties surrounding the state of the mortar and its failure behavior can only be treated, however, with sensitivity studies that are computationally costly. While individual stones comprising the various parts of the bridge (arches, pier, walls, etc.) are not used but rather the combined behavior of the stone and mortar making the finite element mesh (tensile failure controlled by mortar), the distinct parts of the bridge were made out of different segments between which contact conditions (or mortar behavior) control the deformation or failure. Experience has shown (including the Plaka Bridge) that these structures fail in large sections rather individual stones and so the adopted assumption is realistic. For example, the primary arch was represented by twelve (12) different segments connected together with each connection or interface capable of failing or separating under shear or tension (assumed failure criteria for mortar).

Details of the refined FE mesh used to represent the Plaka Bridge are shown in Figure 8.The general finite element mesh-generation software True-Grid [17] and non-linear analysis software LS-DYNA [16] (capable of analyzing static, modal, and earthquake loadings) were employed.

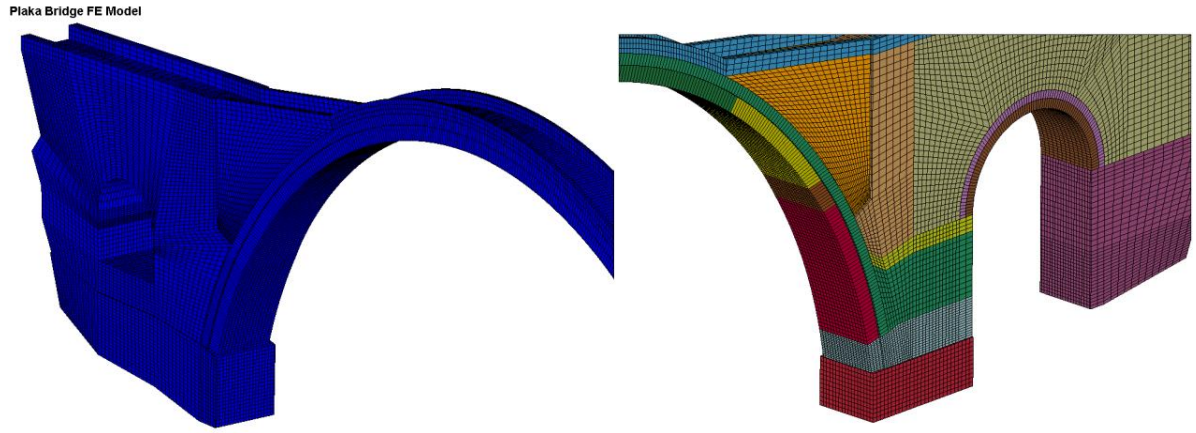

Figure 8: Numerical discretization of the Plaka Bridge into finite elements

4.1 Hydrodynamic Loads

To estimate the hydrodynamic forces on the bridge pier a flow velocity of 8 m/sec has been assumed. The Reynold's number **R** applicable for the pier hydrodynamic forces is ~4.9 10^7. Based on this estimate of **R** it is expected that a boundary layer around the pier will form with the flow (free stream approach velocity) separating at the corners of the pier. Drag forces in the direction of the flow and lift forces acting vertically upwards (combination of buoyancy force $\boldsymbol{VOL}_{\text{submerged\_PIER}} * \boldsymbol{\rho}$)

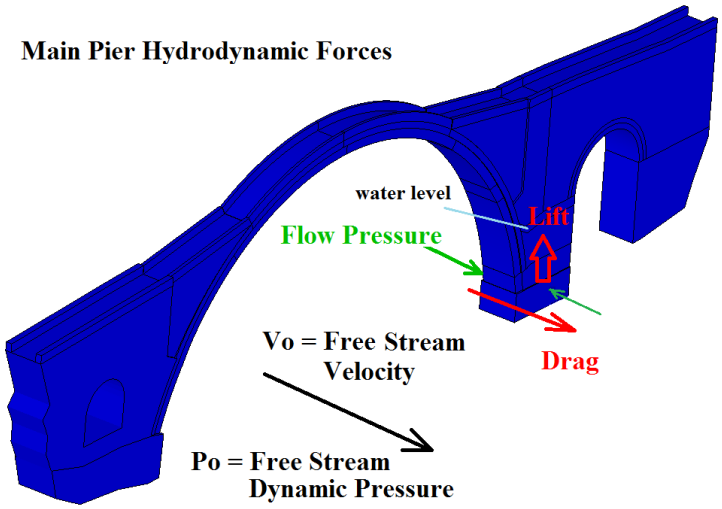

Figure 9: Plaka Bridge schematic and orientation of pier loads

Figure 9 shows characteristics of flow around a bluff body for a high Reynolds number. V_o is the free stream velocity, P_o is the free stream mean dynamic pressure, F_D the drag force on the body, and F_L the lift force on the body.

$$F_{along\_flow} = F_D + (F_{Hy_{upstream}} - F_{Hy_{downstream}})$$

Where $F_{Hy_{upstream}}$ is the hydrostatic force on the upstream face of the pier, $F_{Hy_{downstream}}$ is the hydrostatic force on the downstream face and F_D is the drag force

$$F_D = C_D \frac{1}{2} A_r \rho V_o^2$$

Where C_D is the drag coefficient (~2.0 for the present case), A_r is the reference area (m^2), ρ is the fluid density (Kg/m^3) and V_o the reference flow velocity (m/s). The $F_{\mathbf{Hy\_upstream}} = \boldsymbol{w} \cdot h_{centr} \cdot A_{projected}$ (and similarly the downstream counterpart) is based on the specific weight of water (9, 810 N/m^3), the distance from the free surface to the area centroid (h_{centr}) and the projected submerged area normal to the direction of the flow.

$$F_V = F_L + F_{boyancy}$$

$$F_L = C_L \frac{1}{2} A_r \rho V_o^2$$

C_L is assumed to be ~0.81.

Impact forces generated by moving boulders and impacting the pier have not been considered. Such impact forced can be significant.

4.2 Plaka Bridge Gravity Analysis

Using only gravity loads the Plaka Bridge was analyzed during the first phase of the two-step process. The gravity analysis is a quasi-static one where the structure stabilizes with the help of artificially high global damping. Following the numerical stabilization the phase II was initiated with the application of the hydrodynamic loads using the restart capabilities of the adopted code (LS-DYNA). Figure 10 depicts the boundary conditions for the gravity analysis. Specifically, the bottoms of the central pier as well as the two abutments were assumed fixed on competent rock.

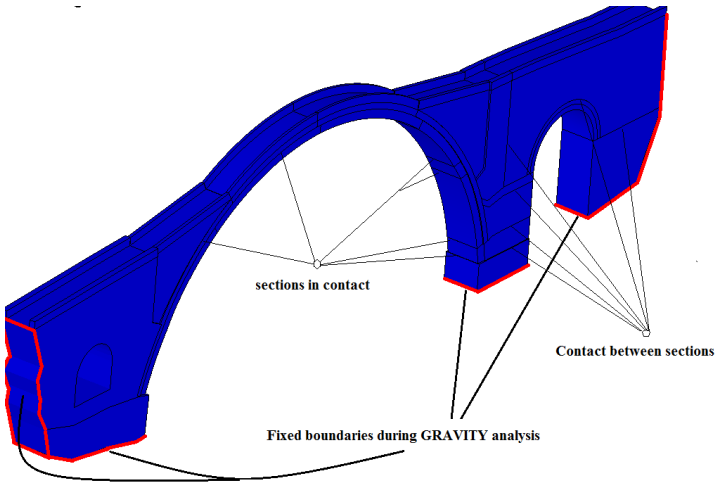

Figure 10: Plaka Bridge boundary conditions for GRAVITY analysis

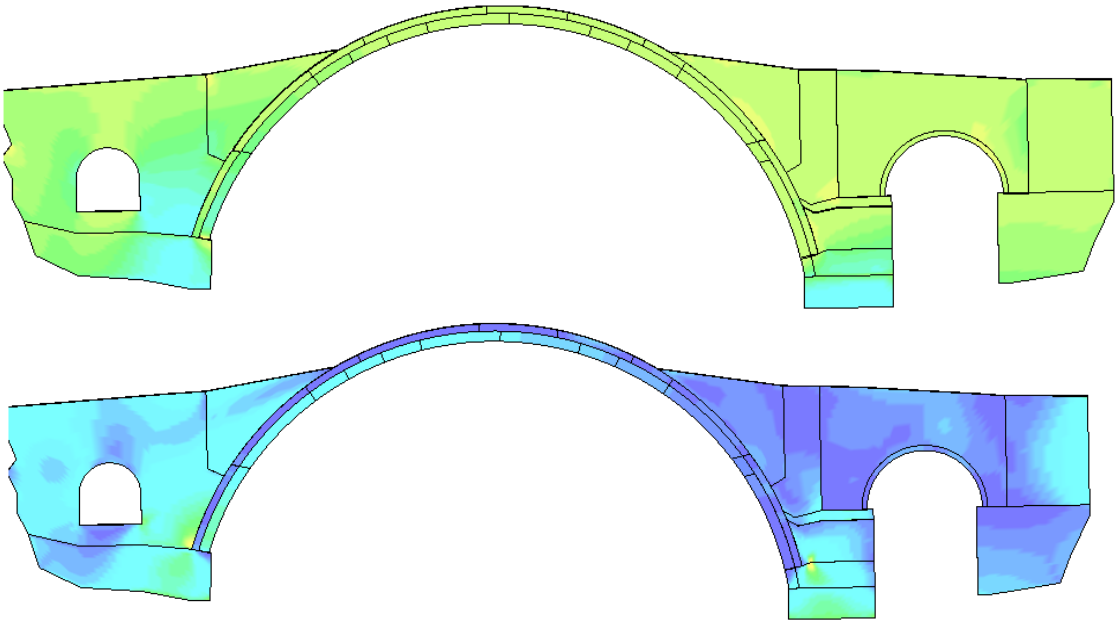

Figure 11: Stress distributions for the Plaka Bridge under gravity load. Vertical stress (top) and principal stress (bottom)

The gravity analysis revealed areas of distress as shown in Figure 12 as well as a confirmation of the need for special ties used in the primary arch.

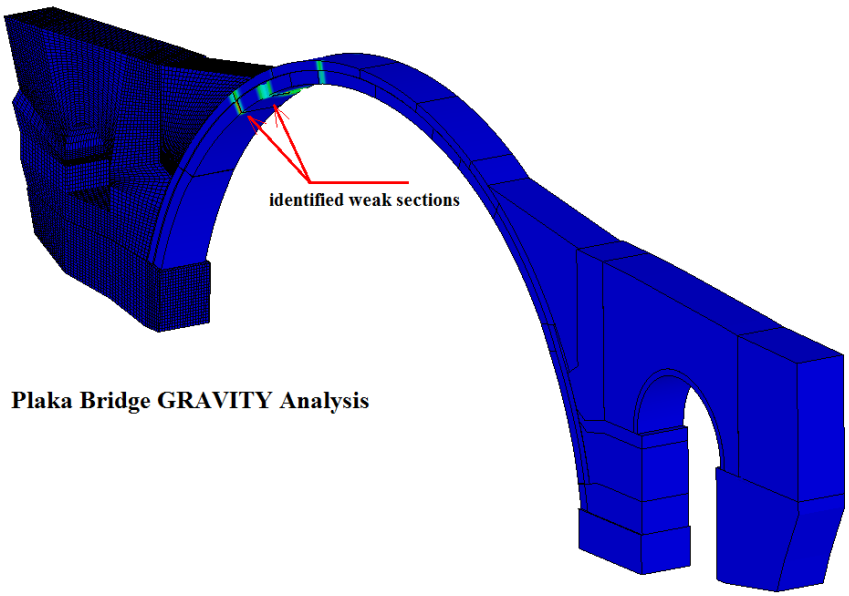

Figure 12: von Mises stresses in Plaka Bridge under gravity load. Important to note is the identification of locations exhibiting high von Mises stresses.


(a)

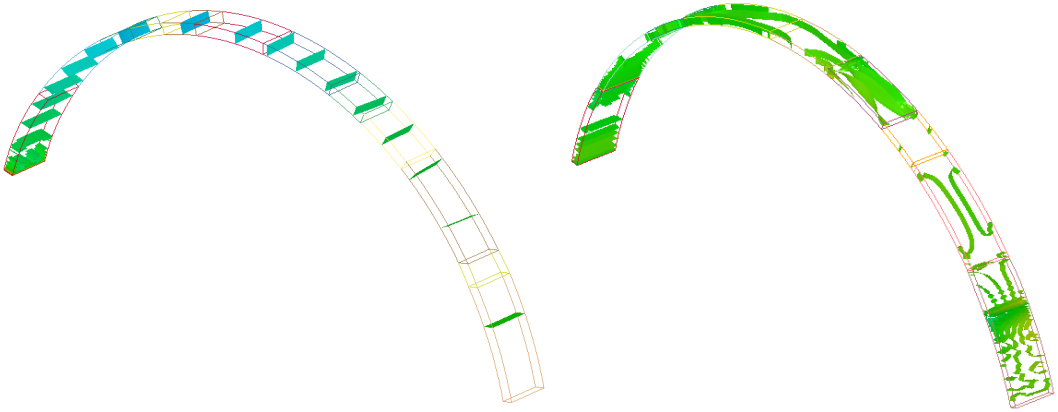

Figure 13: Horizontal stress distribution in the two arches (primary and secondary). The special ties (keys) shown in (a) tend to confirm the need to mitigate forces acting on the primary arch. No such keys are apparently necessary for the secondary arch (as also shown in (a)).

4.3 Plaka Bridge 3D Failure Analysis

Hydrodynamic forces (drag and lift) were distributed on the surfaces up to the level shown in Figure 9. Negative pressure was also assumed (for conservatism) on the downstream face of the central pier.
For the base of the pier, which was assumed to be founded on rock), during Phase II failure conditions were introduced that allowed the bottom of the pier to displace following when the failure conditions with the increasing hydrodynamic loads is met. The hydrodynamic loads built up to the maximum flow assumed and then remained steady. Fixed boundary conditions were assumed for the abutments during Phase II (gravity + flow loads). It was assumed that the river bed was scoured by the flow, exposing the central pier to water flow and pressure all the way to the assumed basement rock.

Shown in Figures 14 and 15 are the early stages of the large deformations exhibited by the Plaka Bridge due to the flood loads. In Figure 14, the separation of large segments of the RHS of the primary arch is observed as the upper structure begins to move in the direction of the flow. Figure 15 (left) a zone of high shear stresses are shown on the LHS of the primary arch and near where the arch structure actually separated from the left abutment (see Figure 3). Figure 15 (right) depicts the large deformation experienced by the lower part of the central pier. While in the postulated failure scenario the base of the pier was intentionally undermined, segments above the base block also begin to move downstream.

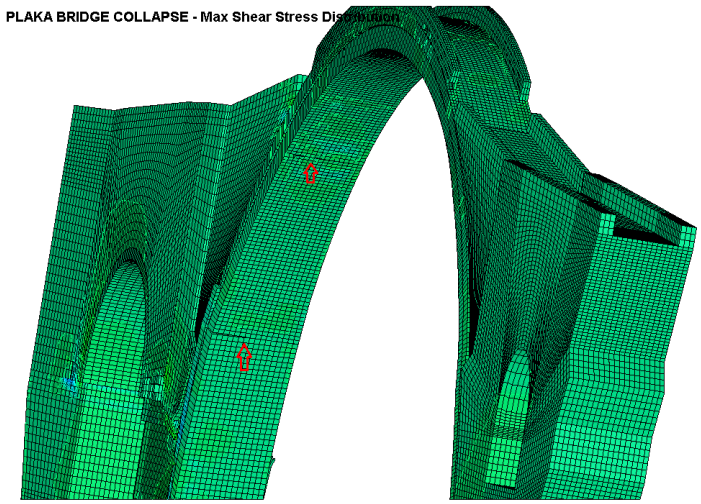

Figure 14: Initiation of collapse with section separation on the primary arch (RHS)

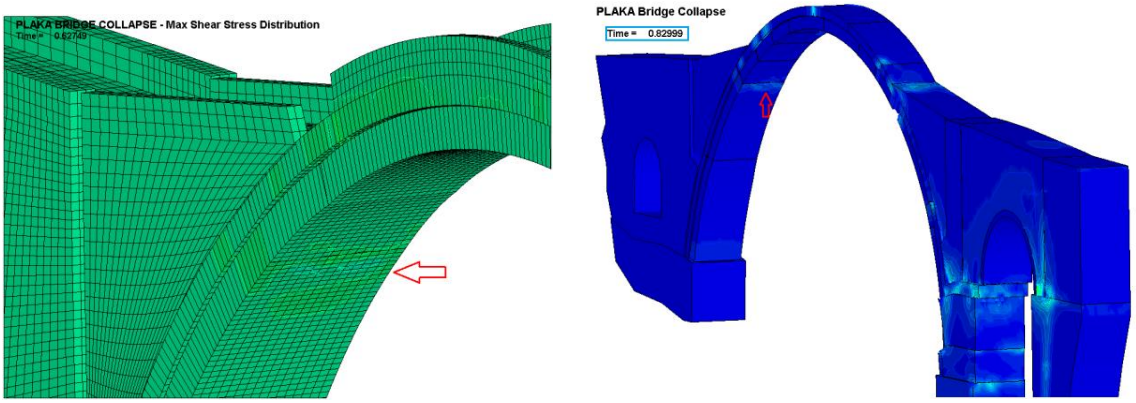

Figure 15: Maximum shear stress profile on the LHS section of the primary arch

The deformation of the primary arch in the early stages of the postulated collapse scenario is shown in Figure 16. Specifically, the evolution of the displacements at locations on the LHS of the arch is shown in Fig. 16 (left). Important to note is the fluctuation of the direction of the arch movement between positive (direction of flow) and negative (upstream). The large displacements of the central pier blocks are also shown in Fig. 16 (right). The rapid fracture occurring in the LHS of the primary arch is depicted in Figures 17 (a-d). Figure 17a depicts the high shear stresses developed on the downstream side of the location and Figure 17b the opening of arch. Important to note is the failure at the location is initiated on the downstream side which indicates that the apex section of the arch exhibits the tendency to move against the flow.

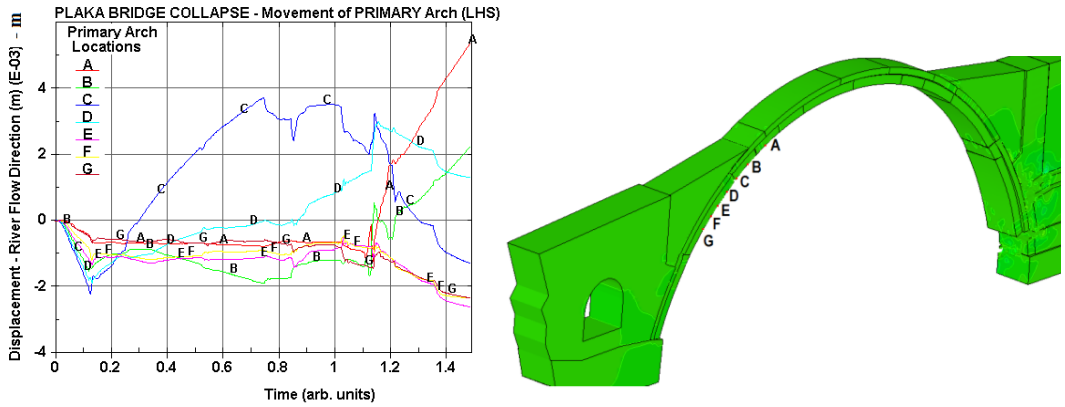

Figure 16: Deformation of the bridge in the early stages of failure

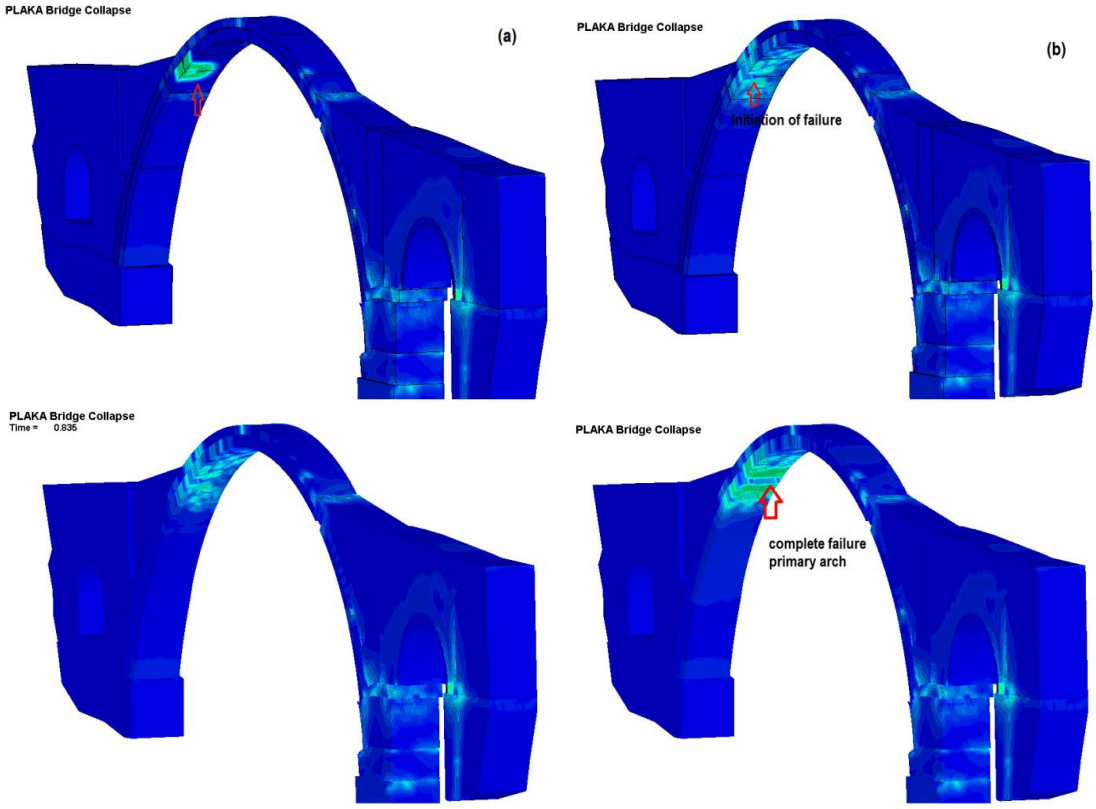

Figure 17: Snapshots of the sudden failure predicted on the LHS of the bridge arch

Figure 18 depicts maximum shear stress distribution during the early stages of the predicted arch failure (location A). Shown is the section (location B) where high shear stresses also develop. Location B represents the RHS location where the right abutment separated from the failed part of the bridge (see Section B-B of Figure 2 and Figure 3).

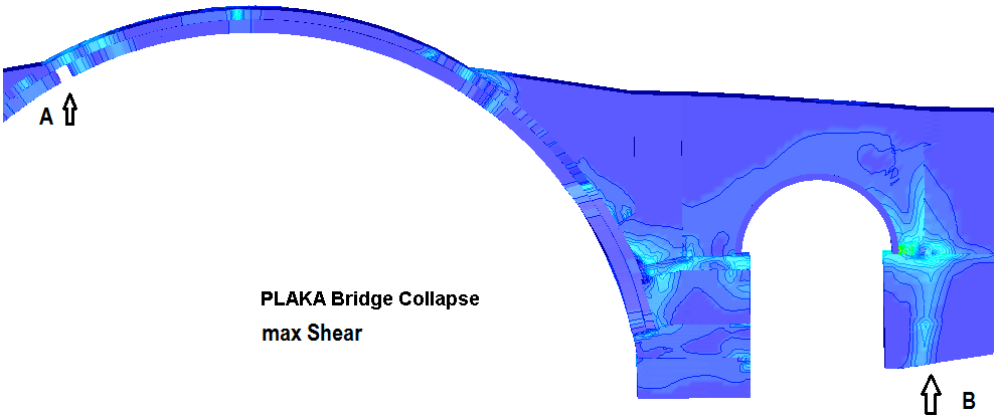

Figure 18: Maximum shear stress profile on the LHS section of the primary arch

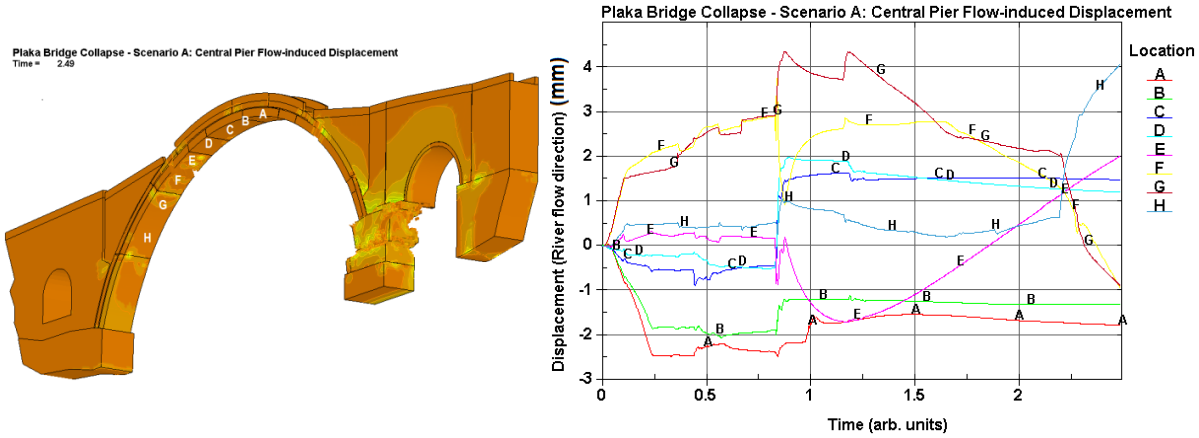

Figure 19: Locations (left) and predicted displacements of the main arch during collapse

The predicted swaying of the arch during the collapse process is clearly depicted in Figure 19 (right) with changes from positive to negative territories of the displacement in the direction of the flow.

Shown in Figures 20 and 21 are stages of the collapse of the Plaka Bridge and the mode of failure of different parts of the bridge that can be used to compare with actual bridge collapse. Two very important observations are made: First, is the predicted mode of failure of the blocks comprising the central pier (Figs. 20d and 21b). This tends to support the observations of the failure in large blocks shown in the photographs of Figures 3 and 4. Second important observation is the rupture surface on the LHS of the arch where it meets the left wall, a location which very close coincides with the actual failure surface (photos of Fig. 3 and 4).

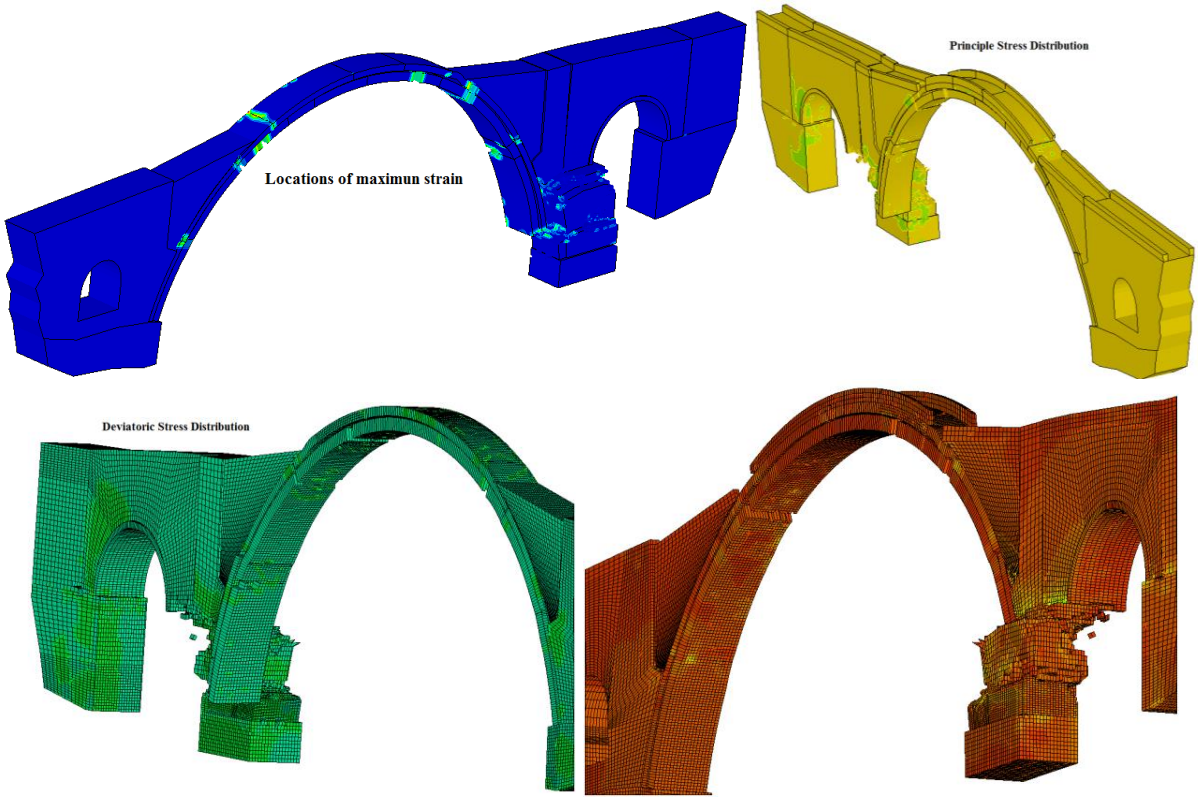

Figure 20: Evolution of collapse (pier) and identification of locations of arch separation.

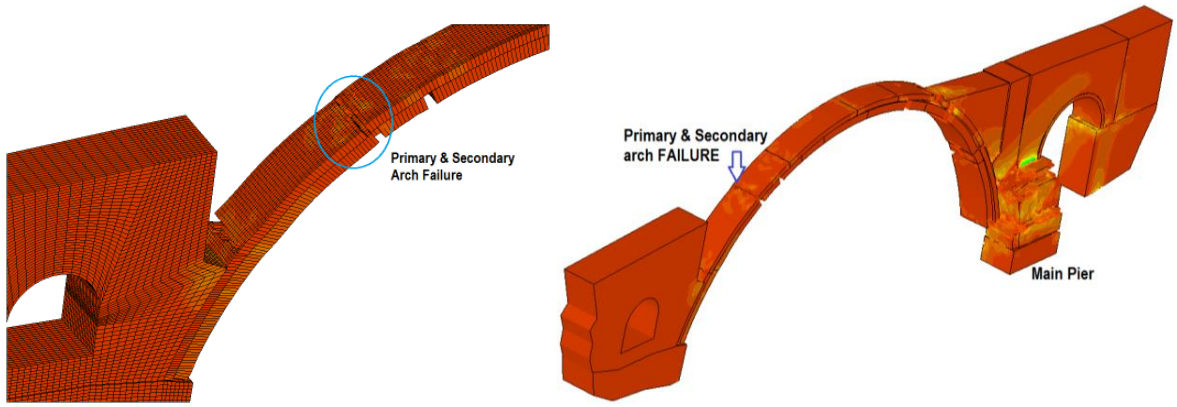

Figure 21: Identification of the location of complete section separation on the LHS of the arch structure (primary + secondary) during the later stages and start of complete collapse. The failure section predicted closely traces the location of the observed failure of the actual bridge (Figure 3).

The state of the structure just prior to the complete collapse and the displacement profile on the LHS of the arch structure where the failure surface has been observed is shown in Figure 22. The displacement indicator ***up***/***dn*** implies displacement in the direction of the flow (dn) and opposite to the flow (up). Delineated is the segment of the secondary arch repaired after the World War II bombing using concrete,

a detail accounted for in the finite element analysis as a potentially influencing parameter when designing failure scenarios.

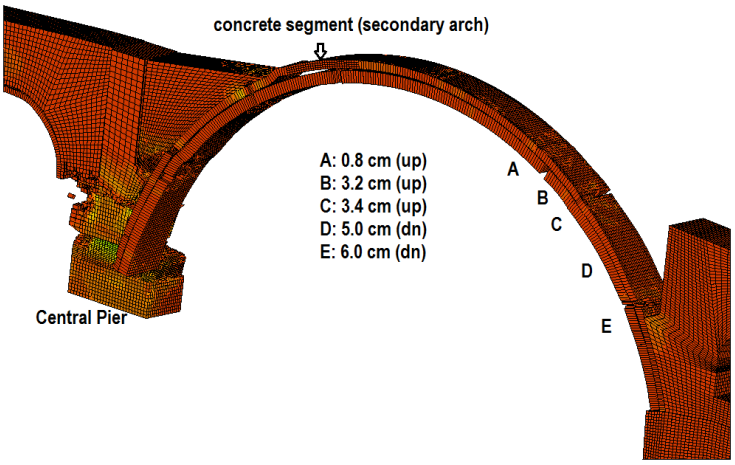

Figure 22: State of damaged Plaka Bridge prior to total collapse and arch deformation profile

5. Summary and Conclusions

A 3D, non-linear finite element representation of the Plaka Bridge was utilized to analyze its February 2, 2015 collapse from unprecedented floods. The two-phase analysis assessed the structure prior to its collapse under gravity loads and simulated a flood load scenario to identify the most-likely cause of the collapse. The structural characteristics and geometry were all accounted for in the numerical representation of the bridge. Material properties for the local stone and the mortar used were deduced from laboratory tests made on actual materials retrieved from the collapsed bridge.

Several scenarios encompassing uncertainties that existed regarding (a) the structural health of bridge prior to the collapse (weakened sections of the arch structure), (b) the conditions at the base of the central pier (competent rock or gravel) and (c) the flow water level were postulated and analyzed. The scenario of the degraded central pier base support (equivalent to the scenario of a weakened pier section above the base) is presented in detail in this paper. This scenario was deemed to be the most likely that has triggered the failure based on the numerical analysis results that seem to corroborate the post failure available evidence. Key, post collapse evidence is summarized in the photographs of Figure 23. Specifically, the following important observations are made based on Figure 23:

- The failure at section A (LHS) appears to have occurred suddenly (as it is evident from the smooth failure surface of the primary and secondary arches).
- A second important point at A (shown in Fig. 23 middle) is the failure surface of the parapet and filling wall. This indicates that the arch section at the LHS location actually separated and fell upstream.
- Figure 23 (right) depicts the orientation of a large segment of the RHS arch structure and wall that was supported by the central pier. The toppling of this large block in the opposite direction than the flow indicates significant rotation resulted from the large displacement of the pier blocks below in the direction of the flood flow.

The numerical analysis and the failure scenario postulated and presented in detail tend to support and corroborate the above evidence regarding the triggering of the collapse and the most-likely cause. It is therefore assessed by the authors, based on the post-collapse evidence and the simulated scenario results,

that the likely cause was the undermining by the flood (scouring of the river bed and hydrodynamic loads) of the central pier.

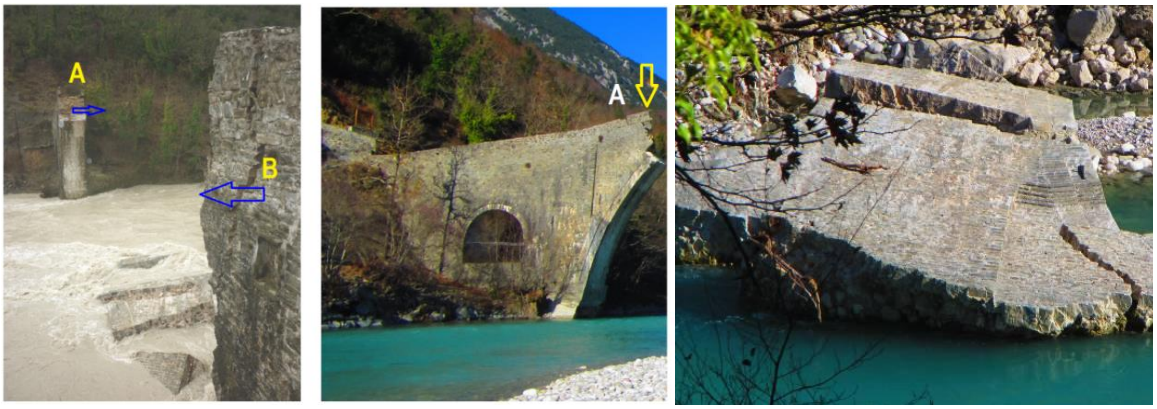

Figure 23: Photographic evidence of Plaka Bridge collapse

In addressing the question whether the collapse was preventable through better engineering interventions and maintenance, or that the historic Plaka Bridge was doomed facing this "*beyond design basis event"* the latter seems to be the most appropriate answer. No maintenance of the superstructure could have prevented its collapse.

The limitation exhibited by the structural materials in enabling the spanning of the river bed with a single arch, forced the builders to use the central pier which was founded on the river bed. Serious uncertainties exist regarding the competence of the foundation and the depth. The combination of the removal of earth pressure on the pier base due to the excessive flood waters and the undermining of the pier support combined with high hydrodynamic loads is believed to be the likely cause of collapse stemming from the location of the central pier. It is the recommendation of the authors that during the reconstruction of the bridge, the exploration of the subsurface and the presence (or not) of competent rock beneath the river bed be fully assessed.

References

1. Manos G.C., Nick Simos N. and Kozikopoulos E. (2016) "The Structural Performance of Stone-Masonry Bridges", Chapter 4, "Structural Bridge Engineering", ISBN 978-953-51
2. N. Simos, G. Manos, E. Kozikopoulos, "Earthquake Vulnerability of Stone Arch Bridges using Non-linear Finite Elements and Measurements of Dynamic Characteristics – A Case Study," *Engineering Structures* (in review), 2016
3. T. Aoki, et al, "Theoretical and Experimental Dynamic Analysis of Rakanji Stone Arch Bridge, Honyabakei, Oita, Japan," 7th International Conference on Motion and Vibration Control, MOvIC 04, 2004
4. J. Kiyono, et al. "Seismic Assessment of Stone Arched Bridges," 15 WCEE, Lisboa, Portugal, 2012
5. B. Sevim et al., "Finite element model calibration effects on the earthquake response of masonry arch bridges," Finite Elements in Analysis and Design, 47, 621–634, 2011

6. N. Simos and G.C. Manos “Numerical Analysis of Seismic Response of Natural Stone Arch Bridges - Field Observations and a Case Study,” COMPDYN 2013, http://www.eccomasproceedings.org/cs2013/
7. Paz. M. International Handbook of Earthquake Engineering: "Codes, Programs and Examples", edited by Mario Paz, Chapter 17, Greece by G.C. Manos, Chapman and Hall, ISBN 0-412-98211-0, 1994.
8. B. O. Caglayan, et al., “Assessment of a concrete arch bridge using static and dynamic load tests,” *Structural Engineering and Mechanics*, Vol. 41, No. 1 (2012) 83-94
9. G.A. Drosopoulos, et al., “Limit analysis of a single span masonry bridge with unilateral frictional contact interfaces,” *Engineering Structures* 28 (2006) 1864–1873
10. Manos G.C. (2011), “Consequences on the urban environment in Greece related to the recent intense earthquake activity”, Int. Journal of Civil Eng. and Architecture, Dec., Volume 5, No. 12 (Serial No. 49), pp. 1065–1090.
11. G. C. Manos, et al., “Field experiments for monitoring the dynamic soil-structure-foundation response of model structures at a Test Site” Journal of Structural Engineering, American Society of Civil Engineers, Special Issue “Field Testing of Bridges and Buildings, D4014012, Vol. 141, Issue 1, January 2015.
12. G.C. Manos, et al., “Numerical Simulation of the Limit Non-Linear Behaviour of Unreinforced Masonry under In-plane State of Stress from Gravitational and Seismic Actions”, COMPDYN 2015, Greece, 25–27 May 2015
13. O’Connor Colin (1993), Roman Bridges, Cambridge University Press, ISBN 0-521-39326-4
14. The stone masonry arch bridges of Greece, Center of environmental education Makrinitsas, ISBN: 978-960-98043-9-4, (in Greek), 2007 http://kpe-makrin.mag.sch.gr
15. K. Psimarni, et al.,“Development of a Geographic Information System for the Traditional Bridges of Central Zagori”, Report to the Municipality of Zagori (in Greek), 2000
16. N. Simos and G.C. Manos “Structural Integrity Assessment of Historical Stone Structures Based on Passive Monitoring of their Dynamic Characteristics,” (in preparation)
17. LS-DYNA - Version 9.71, Livermore Software Technology Corp. – LSTC
18. TrueGrid - Version 2.3.4, XYZ Scientific Applications, Inc